

Article

Wing Design, Fabrication, and Analysis for an X-Wing Flapping-Wing Micro Air Vehicle

Boon Hong Cheaw, Hann Woei Ho *  and Elmi Abu Bakar

School of Aerospace Engineering, Universiti Sains Malaysia, Nibong Tebal 14300, Pulau Pinang, Malaysia

* Correspondence: aehannwoei@usm.my

Received: 28 June 2019; Accepted: 16 August 2019; Published: 20 August 2019



Abstract: Flapping-wing Micro Air Vehicles (FW-MAVs), inspired by small insects, have limitless potential to be capable of performing tasks in urban and indoor environments. Through the process of mimicking insect flight, however, there are a lot of challenges for successful flight of these vehicles, which include their design, fabrication, control, and propulsion. To this end, this paper investigates the wing design and fabrication of an X-wing FW-MAV and analyzes its performance in terms of thrust generation. It was designed and developed using a systematic approach. Two pairs of wings were fabricated with a traditional cut-and-glue method and an advanced vacuum mold method. The FW-MAV is equipped with inexpensive and tiny avionics, such as the smallest Arduino controller board, a remote-control receiver, standard sensors, servos, a motor, and a 1-cell battery. Thrust measurement was conducted to compare the performance of different wings at full throttle. Overall, this FW-MAV produces maximum vertical thrust at a pitch angle of 10 degrees. The wing having stiffeners and manufactured using the vacuum mold produces the highest thrust among the tested wings.

Keywords: bio-inspired; flapping-wing; wing design; micro air vehicle; thrust measurement

1. Introduction

Micro Air Vehicles (MAVs) are now an active research focus that have caught the attention of global talents. The US Defense Advanced Research Project Agency (DARPA) defined the physical size of an MAV to be not more than 15 cm (usually referred to as a Reynolds number less than 10^5), and the maximum weight to be less than 100 g [1]. This definition, however, is not widely applied by all researchers because, until today, there have been technological limitations to produce smaller electronics and materials for MAVs within the defined sizes. Hence, to invent MAVs that can mimic natural flyers using the smallest possible manufactured parts, researchers usually do not observe a strict size limit when designing their MAVs.

In general, there are three vehicle concepts: Rotary-wing, flapping-wing, and fixed-wing. They have been used according to their advantages and disadvantages. Since fixed-wing MAVs are able to fly for a longer period of time, they have been widely used for surveillance, which requires a long-distance flight with proper planning [2]. On the other hand, rotary-wing MAVs have hovering and vertical take-off and landing capabilities, so they have been extensively used in aerial photography and package delivery [3]. Fixed-wing and rotary-wing design have been observed to suffer from degraded aerodynamic performance when downsizing the model [4]. It has been highlighted that fixed-wing MAVs encounter fundamental challenges with a low lift-to-drag ratio and unfavorable flight control [5]. Compared to rotary-wing MAVs, flapping-wing Micro Air Vehicles (FW-MAVs) are well-known for their effective flight performance and hovering capability [6]. FW-MAVs are small, allowing them capable of operating in a confined environment. Moreover, they produce less noise compared to the rotary-wing design, meaning they have low detectability and are perfect for surveillance purposes [1].

Based on the inspiration of biological flyers in nature, ornithopter-type MAVs have been split into two main categories: Bird-inspired FW-MAVs and insect-inspired FW-MAVs. Both designs fly by flapping their wings but fundamentally differ from each other in many ways [7], including in terms of wing kinematics and control mechanisms. Insect-inspired FW-MAVs have become a rising trend for researchers to develop various prototypes due to their higher degrees of complexity in flight kinematics and capability of flying at low forward speed or even hovering in an extremely low Reynolds number flow condition without stalling. Unlike insect-inspired FW-MAV, bird-inspired FW-MAVs require an initial launching speed while flapping their wings to produce lift and propulsive thrust to fly and stay aloft in the air.

Natural flyers use their wings as a lift-generating mechanism to stay aloft. One of the wing kinematics is clap-and-fling. This technique suggests that wings are slapped together then flung apart at the end of each stroke [8]. As a result, a bound vortex is formed on each wing edge, which remains attached until the next stroke, thus inducing circulation on the wing, creating a pressure differential and encouraging high values of lift [1]. Other unsteady aerodynamic mechanisms, such as wing leading vertex and delayed stall [9], wing rotation [10], and wake capture [11], also contribute to lift generation in FW-MAVs. The first insect-sized FW-MAV invented was named Harvard Robobee [12]. The high speed, highly articulated mechanisms that are necessary to replicate an insect-like wing flapping motion exists on a scale that is between microelectromechanical systems (MEMS) [13] and “macro” devices [14]. Hence, a “meso” scale rapid fabrication method, the so-called smart composite microstructures (SCMs), were used to fabricate the Robobee. With only 0.06 g and 3 cm of wingspan, this FW-MAV has achieved 3–4 min tethered-hovering flight with a flapping frequency of 110 Hz and a maximum speed of 6 m/s.

Until today, only a few research teams have successfully demonstrated a controlled flight of an insect-like FW-MAV [15–17]. AeroVironment has spent five years in a project financed by DARPA, the so-called Nano Hummingbird, one of the few notable platforms which is capable of untethered hovering flight [15]. It is regarded as a huge breakthrough in FW-MAVs research because of its gyroscopically-stabilized flight without any tail control surfaces. Similarly, KUBeetle, a 21 g two-winged tailless MAV flaps at a frequency of 30 Hz and is capable of taking off, hovering and loitering [16]. DelFly variants have also achieved a remarkable flight performance: DelFly II can attain a high thrust-to-power ratio [17]. The most recent breakthrough is a tailless DelFly variant, DelFly Nimble, designed by Micro Air Vehicle Laboratory (MAVLab) at Delft University of Technology [18]. The MAV can hover or fly in any direction (up, down, forward, backward or sideways).

Figure 1 (DelFly Nimble), Figure 2 (KUBeetle), and Figure 3 (NUS FlowerFly) reveal the location of electronics components along the fuselage in the longitudinal view. In general, the flapping gearing mechanical systems and motors are always located at the nose of the aircraft. For DelFly Nimble and KUBeetle, there are also servos located at the nose of the MAV for control mechanisms. These FW-MAVs also share a similarity, in which the autopilot, electronic speed controller (ESC) and radio receiver are located in the middle section of the fuselage and usually the aft of the wing structure. After that, at the rear section of the FW-MAVs the battery and remaining servos are located. This study has provides an insight into the electronics positioning on FW-MAVs. It is noted that the passive longitudinal stability can be achieved by carefully shifting the position of the battery, ESC, and radio receiver along the fuselage.

Although these FW-MAVs have shown their capabilities with different setups, there are many challenges remaining including design, fabrication, control, and propulsion. To this end, this paper investigates the wing design and fabrication of an X-wing FW-MAV and evaluates its vertical thrust generation. Some related works have been carried out to examine the effect of different wing designs of FW-MAVs on thrust generation [19–21]. A comprehensive study with experiments was conducted to investigate the thrust generation and power consumption of different wing configurations and motions for a hovering FlowerFly [19]. The results showed that, at the same flapping frequency, the less flexible wing leading edge can produce more thrust. Additionally, a wing configuration with the highest

thrust-to-power ratio or power loading was determined from the experiments. Another study on KUBeetle was made to examine the power loading of different deformable wing configurations with several vein placements [20]. Both theoretical and experimental results showed that an additional outboard vein on the wing can further reinforce the wing membrane and, thus, can perform better in terms of power efficiency. A design optimization of the wing of a FW-MAV has been carried out by varying its camber angle, aspect ratio, taper ratio, and surface area [21]. This study concluded that some critical parameters, such as the camber angle and aspect ratio, have a significant impact on the thrust generation, and the combination of a trapezoidal wing and a straight leading edge achieved the best performance. Inspired by these works, we conduct a preliminary study on the investigation of the vertical thrust generation of three different wings of an X-wing FW-MAV at different pitch angles. From this study, we determine the wing that can achieve the best result in terms of thrust generation, and at which angle the FW-MAV can produce the maximum thrust.

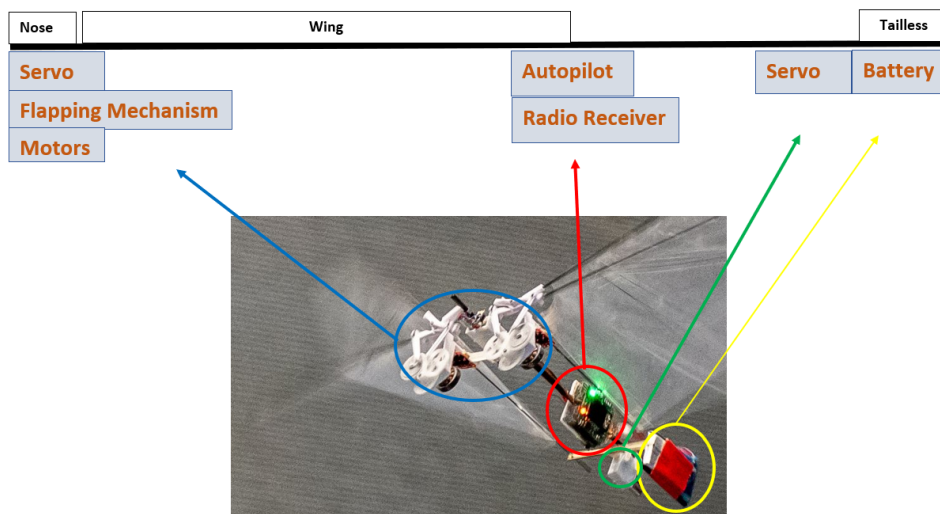


Figure 1. Electronic components' location in the DelFly Nimble [18].

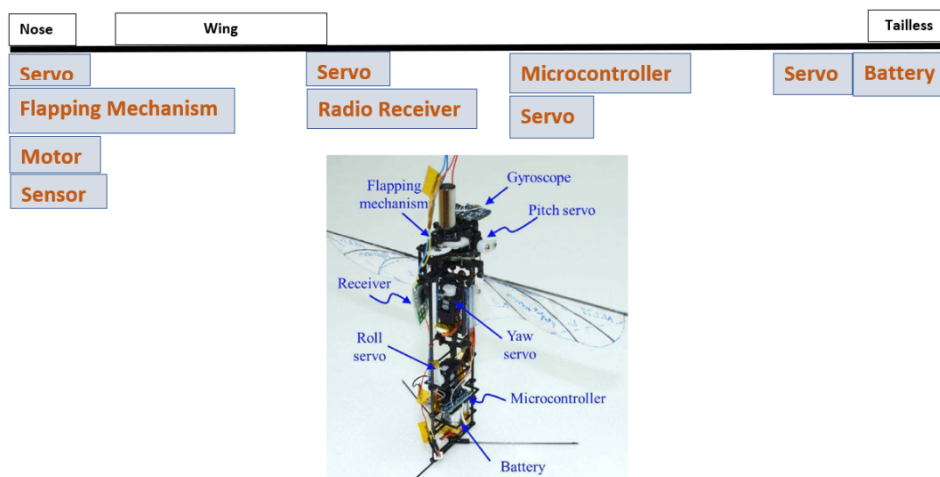


Figure 2. Electronic components' location in the KUBeetle [16].

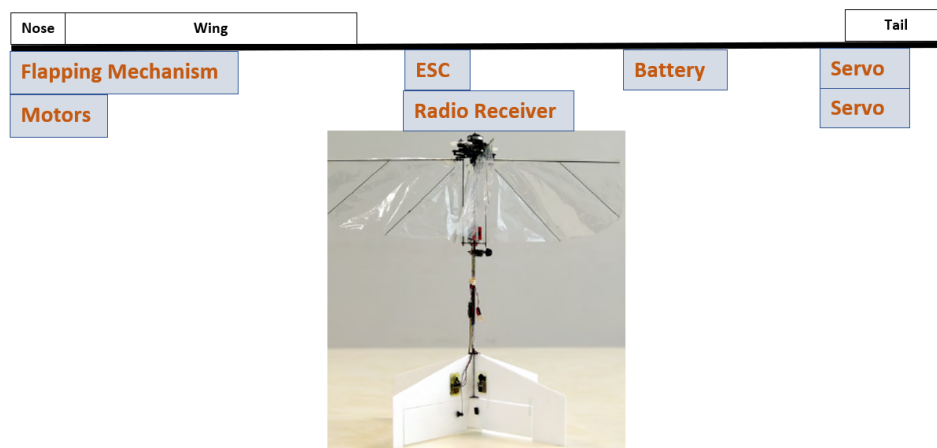


Figure 3. Electronic components' location in the NUS FlowerFly [19].

2. Wing Design and Fabrication

In this section, the methodologies of wing design, fabrication, and analysis are discussed. A systematic approach to estimate the wing design parameters is introduced. Two wing fabrication methods for FW-MAVs are also presented, and a performance analysis that examines the thrust generation of the wings is described in this section.

2.1. Wing Sizing Method

Wing sizing method comprises five steps which eventually estimate the important parameters for the final wing design. These steps are presented in the subsections below.

2.1.1. Step 1—Defining the Flight Parameters

In this study, the FW-MAV will be flying in an indoor environment at a known latitude, L_0 , and altitude, h_0 . The latitude and altitude are used to calculate the gravitational acceleration, g , at the place where the FW-MAV is flying. Based on the mission, the relevant flight class of the flapping wing is determined. Then, as part of the flight planning, the mission will be analyzed including extracting the atmospheric parameters (i.e., air temperature, air density, kinematic viscosity, air pressure, and acceleration of gravity) of the flight zone, and determining the distances and flight time. These parameters will be used to estimate the FW-MAV cruise speed, Reynold's number, and other flight parameters.

2.1.2. Step 2—Defining the Flight Modes

The flight modes will be determined in this step. Generally, for an aircraft, the modes consist of different stages, including take-off and landing, cruising, turning, climbing, and descending. For the FW-MAV used in this study, the flight modes are take-off, forward flight, hovering, and turning.

2.1.3. Step 3—Selecting the Wing Parameters

After completing Step 2, the best wing shape and its aspect ratio will be selected. This can be done by studying the existing FW-MAV's wing design and its performance with different aspect ratios. Experiments to study the effect of different wing parameters on flapping-wing performance have been carried out with the objectives being to optimize wing shape and wing geometry for the FW-MAVs [21]. From the study, a wing in a trapezoidal shaped with an aspect ratio of 3.50 (for a complete wing), a taper ratio of 0.552, and stiffener locations of 84° and 35° gives better thrust characteristics [22]. Besides, it is also mentioned that wings with larger aspect ratios gain a higher lift to drag ratio, which is similar to the common rules used in fixed-wing aircraft [23]. In conclusion, the aspect ratio AR used for this paper is 3.50 (for a complete wing) and the taper ratio λ , is 0.55.

2.1.4. Step 4—Determining the Parameter of Wing Loading

Using the atmospheric parameters in Step 1, the required flight parameters to estimate the FW-MAV’s wing loading have to be calculated in the first place. These values are used to complete the equations of thrust loading ($\frac{T_{SL}}{W}$) as a function of wing loading ($\frac{W}{S}$) for different flight modes in Table 1. At this point, a constraint analysis should be conducted. The constraint equations for different flight conditions are derived from the master equations called Mattingly’s method [24], as presented in Table 1. The thrust loading ($\frac{T_{SL}}{W}$), as presented in Equation (1), is a function of wing loading ($\frac{W}{S}$). Therefore, by drawing the related curves using Equations (2)–(7), a bounden space to determine a design point ($\frac{W}{S}, \frac{T_{SL}}{W}$) can be obtained. The design point should satisfy all the constraints according to the defined mission. The wing loading which satisfies all constraint will be used after Step 5 to calculate the required wing surface area.

$$\frac{T_{SL}}{W} = \frac{1}{\alpha} \left\{ \frac{qS}{W} \left[k_1 \left(\frac{nW}{qS} \right)^2 + 2\psi C_f \right] + \frac{1}{U} \frac{dZ}{dt} \right\}, \tag{1}$$

where

$$\alpha = \frac{T_a + 273.16}{T_a + 273.16 - 0.001981h_0} \left\{ 1 - \frac{0.001981h_0}{288.16} \right\}^{5.256},$$

$$k_1 = \frac{1}{\pi e AR}, e = \text{oswald efficiency factor},$$

$$q = 0.5\rho U_{ref}^2, U_{ref} = \text{local reference velocity},$$

$$\psi = \frac{\text{ratio of the parasite drag coefficient of flapping wing}}{\text{frictional drag coefficient for a flat sheet}} \text{ (value between 2 – 4.4),}$$

$$C_f = 0.455 (\log_{10} Re)^{-2.58}, Re = 10^5, \text{ according to definition of MAVs}$$

$$Z = h + \frac{U^2}{2g}, \text{ and}$$

$$U = \text{Velocity} = \frac{\text{distance travelled, } d}{\text{total time, } t}.$$

Table 1. Thrust loading equations used at different flight conditions.

Flight Condition	Equation
Case 1—Constant Altitude/ Speed Cruise	$\frac{T_{SL}}{W} = \frac{1}{\alpha} \left\{ \frac{qS}{W} \left[k_1 \left(\frac{W}{qS} \right)^2 + 2\psi C_f \right] \right\}$ (2)
Case 2—Constant Climb Speed	$\frac{T_{SL}}{W} = \frac{1}{\alpha} \left\{ \frac{k_1 W}{qS} + 2\psi C_f \frac{qS}{W} + \frac{1}{U} \frac{dh}{dt} \right\}$ (3)
Case 3—Horizontal Acceleration	$\frac{T_{SL}}{W} = \frac{1}{\alpha} \left\{ \frac{k_1 W}{qS} + 2\psi C_f \frac{qS}{W} + \frac{1}{g} \frac{dV}{dt} \right\}$ (4)
Case 4—Sustained turn/ Constant turning altitude	$\frac{T_{SL}}{W} = \frac{1}{\alpha} \left\{ k_1 n^2 \left(\frac{W}{qS} \right) + 2\psi C_f \frac{qS}{W} \right\}$ (5)
Case 5—Service Ceiling/ Accelerated Climb	$\frac{T_{SL}}{W} = \frac{1}{\alpha} \left\{ \frac{k_1 W}{qS} + 2\psi C_f \frac{qS}{W} + \frac{1}{U} \frac{dh}{dt} \right\}$ (6)
Case 6—Hand Launch Stall Speed	$\frac{W}{S} = \frac{1}{2} \rho U^2 C_{Lmax}$ (7)

2.1.5. Step 5—Estimating the Electrical and Structural Weights of FW-MAV

In general, the total weight of the FW-MAV is the sum of structural weight, W_{Str} , and electrical components’ weight, W_{Eq} . W_{Eq} is the total weight of the battery, payload (such as sensors), avionic system (such as servo motors, receiver, microcontroller), and power plant (such as motors and ESCs). Thus, W_{Eq} can be accurately measured using a micro weighing scale. W_{Str} is the total weight of the wing, tail, fuselage, gearbox system, and other parts. To estimate W_{Eq} , a statistical method is

used [25,26]. From Table 2, there are three distinct groups to be considered according to the weight of FW-MAV. Each of the weight constituents as a percentage for these groups are presented.

Table 2. Percentage of the weight of the constituents of flapping wings for the three weight classes.

Weight Range (g)	$W_{PP}(\%)$	$W_{PL}(\%)$	$W_B(\%)$	$W_{AV}(\%)$	$W_{Str}(\%)$
<100	23	2	24	13	38
100–400	16	1	14	9	60
400–800	12	0	12	4	72

In this paper, we will consider a weight range that is below 100 g. Notice that we can estimate the structure weight of the FW-MAV using the percentage reference, that is, 38%. After that, the total weight of FW-MAV can be estimated. After the total weight and the wing loading values are obtained from Step 4, the total wing area can be calculated using Equation (8).

$$S_w = \frac{W_{TO}}{\text{Wing loading obtained from Step 4}}. \quad (8)$$

Thus, the wing span b , wing mean chord C_w , root chord C_r , and tip chord C_t for the wing can be calculated using Equations (9) and (10):

$$\text{Aspect Ratio, } AR = \frac{b^2}{S_w} = \frac{b}{C_w}. \quad (9)$$

$$\text{Taper Ratio, } \lambda = \frac{C_t}{C_r}. \quad (10)$$

2.2. Wing Fabrication

After obtaining the wing size, the wing prototypes can be fabricated using the so-called traditional and advanced methods with a suitable material. A thrust measurement setup is proposed to measure the performance of the fabricated wings.

2.2.1. Wing Materials

The material used for fabricating the wing is one of the major key elements as it has a significant effect on the overall performance of FW-MAVs. The materials selected to fabricate the wings were 15 μm polyethylene terephthalate (PET) films, 0.5 mm carbon rods for stiffeners, and 1.0 mm carbon rods for leading edges. A depron foam sheet was used to make the tails because of its lightweight characteristic. For the fuselage, a 1.4 mm square carbon tube was used.

2.2.2. Wing Fabrication Using Traditional Method

The first method to manufacture the wings was a traditional cut-and-glue method, as shown in Figure 4. It is the simplest and fastest method used to fabricate flapping wings. First, a 2D drawing with the contours of wing was printed on an A3 size paper with the actual size. The drawing was then pasted on a clean table using a transparent single-sided tape, and all corners were sealed properly (Step 1). Next, a piece of 15 μm thickness PET film that is bigger than A3 size was secured on top of the 2D drawing using the same tape. The PET film was used because of its good tensile strength (not deformed easily) and good optical clarity. The PET film should be taped in a way that the film will not be too loose or too tight to prevent the wing suffering from poor thrust generation (Step 2).

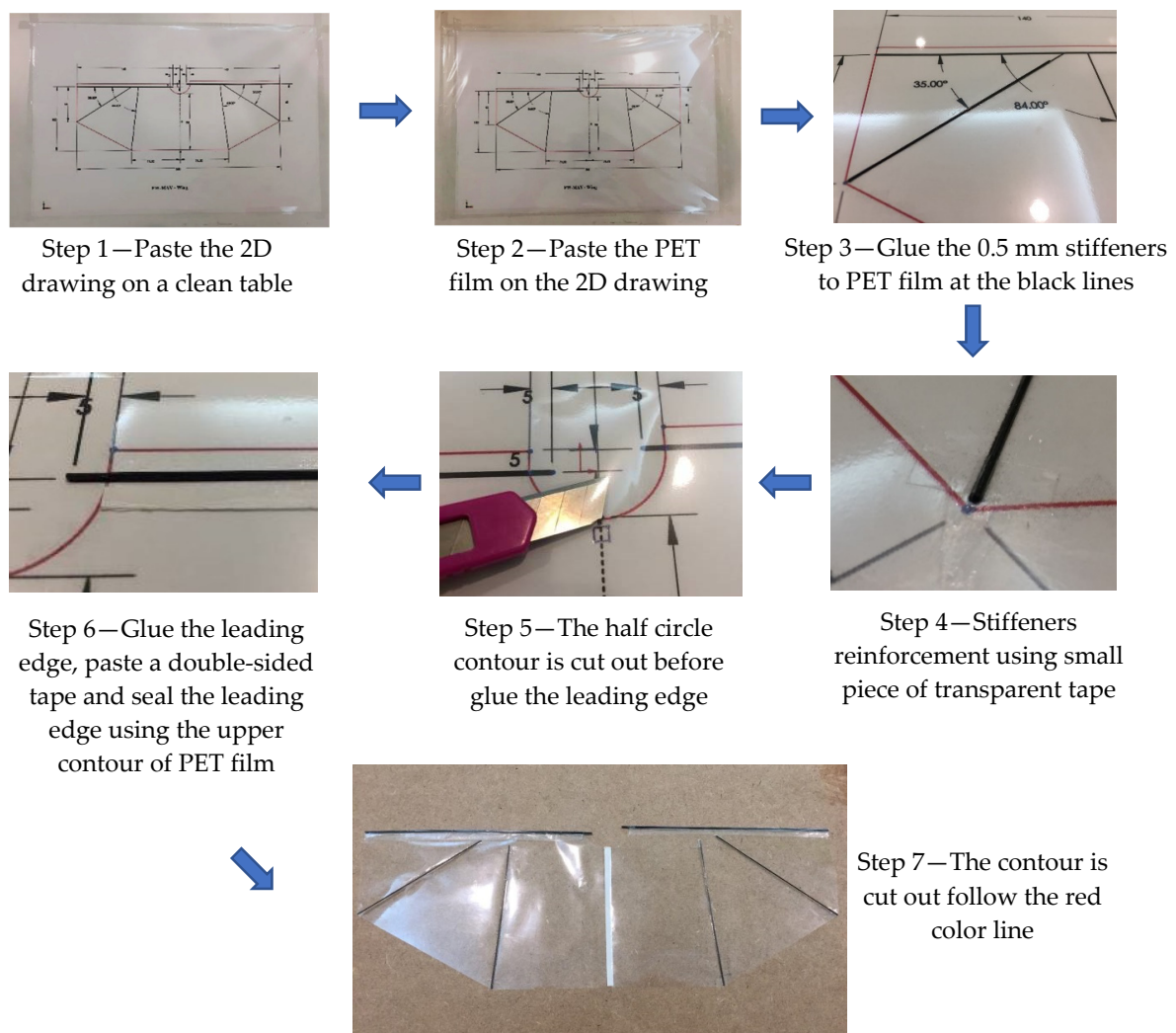


Figure 4. Procedure of fabricating the wing using the traditional cut-and-glue method.

After that, the stiffeners were adhered using an instantaneous glue onto the PET film at four different black lines within the wing contour, as shown in the 2D drawing (Step 3). The stiffeners used were small carbon rods with a diameter of 0.50 mm that were cut to the appropriate length (i.e., 85.0 mm, 90.0 mm, 93.0 mm, 95.0 mm). The glue was slowly dropped onto the stiffeners, which were held vertically to reduce the amount of glue applied on the wing film and minimize the wing mass. After the entire stiffener was covered with the glue, it was quickly placed in the right position before the glue hardened. The next step (Step 4) in this fabrication process was to reinforce both ends of the stiffeners (i.e., near the leading edge and trailing edge). The purpose of conducting this reinforcement was to prevent the stiffeners from detaching from the wing film during flapping. The transparent tape was cut into a smaller size that just fit to paste on top of the stiffeners end to the wing film.

Since the leading edge carbon rod will later slot in the gearbox system, and it is difficult to remove the glue from carbon rod, the ellipse or semi-circle shaped wing contour has to be cut out first before adhering the leading edge on the PET film; this can help prevent the carbon rod from sticking to the ellipse film (Step 5). Using the same glue, the leading-edge carbon rods can be adhered onto the wing film (Step 6). The size of the carbon rod used for the leading was 1.0 mm diameter and 140.0 mm length. After the glue hardened, the top contours, which were 5 mm away from the 1 mm diameter carbon rods, were cut. The next step was to paste a thin double-sided tape on the PET film area just below the 1 mm carbon rods. Once the tape cover was removed, the top contour was slowly pushed and pasted onto the tape area. This covers the 1 mm carbon rod and forms a stronger adhesion between the

carbon rod and PET film. Finally, the rest of the wing contour was carefully cut out and the first wing was complete (Step 7). The above procedure was repeated for another pair of wings to complete the biplane wing configuration. The excess glue on the carbon rods can be removed by putting them into a solvent, such as acetone.

2.2.3. Wing Fabrication Using Advanced Method

This method requires a vacuum mold and a vacuum generator. Figure 5 shows the 2D drawing of the mold design. Two pieces of medium-density fiber boards (MDF boards) of 1.8 cm and four rectangular MDF bars were prepared to manufacture the vacuum mold. The specific dimensions of the MDF boards and bars are shown in Table 3.

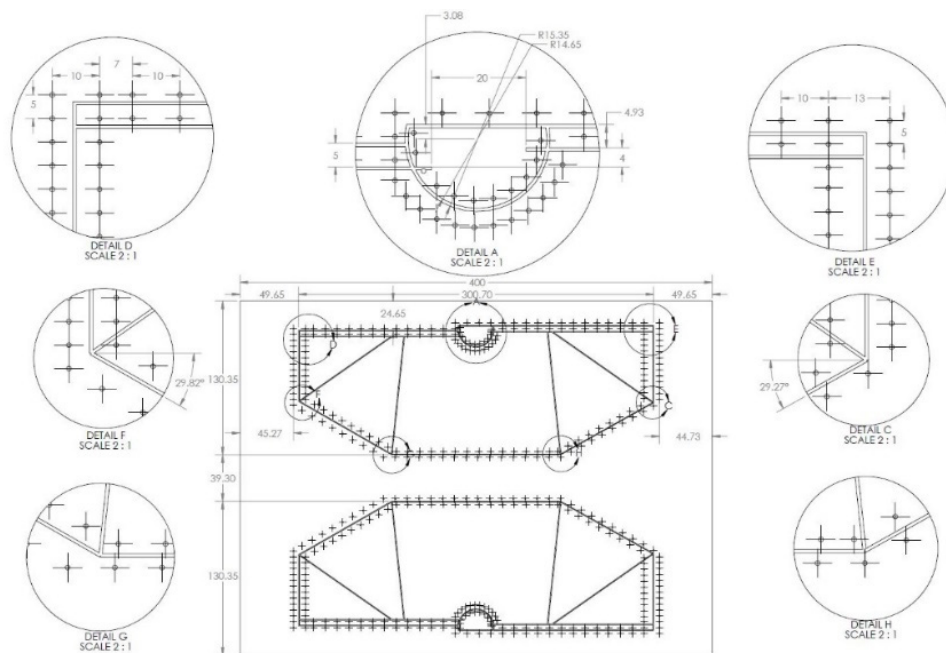


Figure 5. 2D drawing of the vacuum mold to be milled on MDF board.

Table 3. MDF board and bars dimension.

Picture	Name	Dimensions	Amount
	MDF Board	30.0 cm × 40.0 cm	2
	MDF Bar (Long)	38.2 cm × 2.0 cm	2
	MDF Bar (Short)	28.2 cm × 2.0 cm	2

One of the MDF boards was milled into a wing shape mold using a CNC high speed milling machine. The dimension of the mill tool used in milling the wing contour was 0.7 mm diameter, which creates a 0.3 mm depth on the surface. When the milling was finished, holes of 1 mm diameter on both the inner and outer sides of the wing contour were drilled straight through the MDF board. The purpose of these drilled holes is to keep the PET film sticks on the MDF mold under a vacuumed condition. It was ensured that the holes were consistently 1 mm because the vacuum suction force could deform or tear the PET film. Figure 6 shows the MDF board after the milling and drilling processes.



Figure 6. The MDF mold after milling and drilling.

The rest of the materials were used to make the vacuum box. A 10 mm diameter hole was drilled on the 38.2 cm MDF bar so that the hose from vacuum generator could be connected to the mold. The MDF bars were then arranged and pasted on the edge of another piece of the MDF board using the glue as shown in Figure 7. The mold and the vacuum box were combined and sealed using masking tape. Figure 8 shows the full assembly of the flapping wing vacuum mold with the vacuum generator (i.e., a 10 Pa ultimate vacuum pressure).

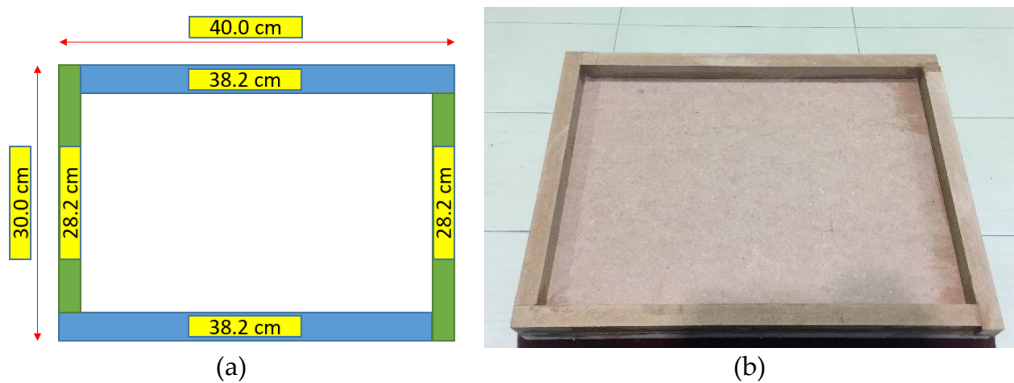


Figure 7. The MDF vacuum box. (a) The dimension of the MDF vacuum box and (b) The actual MDF vacuum box.

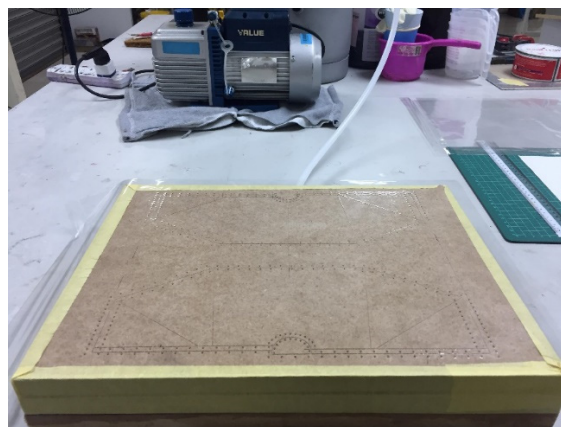


Figure 8. The assembly of the MDF mold and the vacuum generator.

After the setup was complete, the vacuum generator was switched on and the PET film was placed onto the MDF mold. The PET film was checked to be smooth and free of any trapped air bubbles and wrinkles. After that, the wing was fabricated using the procedure presented in the traditional method,

starting from Step 3. Although the steps to fabricate the wing are almost the same, there are several extra steps that need to be taken. Firstly, the vacuum generator has to be activated throughout the fabrication process to make sure that the tension of the film is consistent, which is not too tight and not too loose. Secondly, a pushing force should be applied when pasting the carbon rods onto the groove areas to allow more bonding surface areas between the carbon rods and the PET film. Figure 9 shows an example of the PET film adhered with the stiffeners on the vacuum mold.

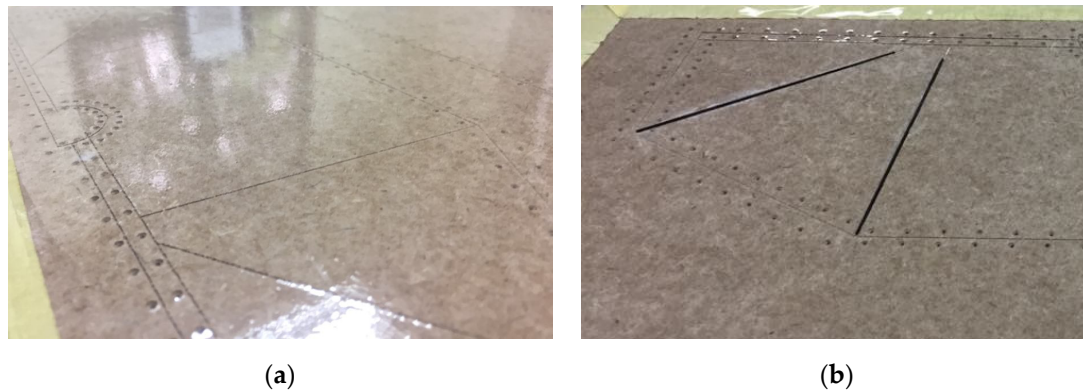


Figure 9. A PET film on the vacuum mold. (a) A PET film on the vacuum mold setup and (b) The stiffeners are adhered on the PET film at the groove areas.

2.3. Vertical Thrust Measurement Setup

The thrust generated in the vertical direction by the FW-MAV, or the so-called vertical thrust, is essential as it allows the MAV to carry its own weight and the weight of other payloads. To obtain the vertical thrust, a load cell setup that estimates a load in grams was needed. Figure 10 illustrates the relationship between the vertical thrust and lift.

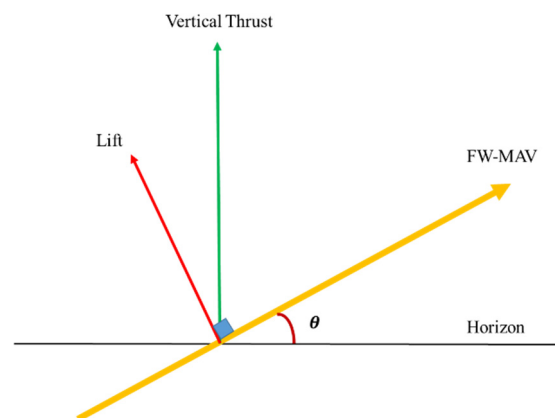


Figure 10. The relationship between vertical thrust and lift of the flapping-wing Micro Air Vehicle (FW-MAV).

Using pinewood sticks, 3 mm bolts, nuts, washers, and a stainless-steel L-shaped plate, a jig that can mount the FW-MAV and adjust different angles was fabricated and is shown in Figure 11a. The load cell model used was a 5 kg straight bar load cell with an HX711 amplifier module, which has a sensitivity of 0.017 g per serial output, as presented in Figure 11b. To begin with the measurement, the pinewood jig was mounted on the load cell setup. The FW-MAV was then mounted at the T-shaped pinewood, as shown in Figure 11c. Next, the load cell HX711 Arduino driver was integrated into an Arduino Uno, and the load cell reading was calibrated before taking any measurement. The measurement began by connecting the load cell, as shown in Figure 11d. Then, after waiting for 10 seconds the throttle was pushed to the maximum (i.e., maximum flapping frequency). One measurement was

taken after obtaining 30 vertical-thrust readings and disconnecting the load cell and saving the data. The measurements were repeated at pitch angles from -60° to 120° , as shown in Figure 12.



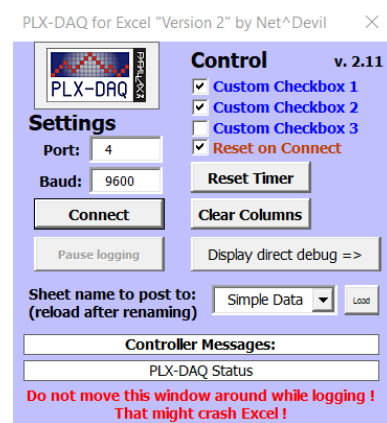
(a) T-shaped jig with a rotating mounting of the FW-MAV



(b) A 5 kg straight bar load cell with HX711 amplifier module



(c) The completed setup of vertical thrust measuring load cell setup



(d) PLX-DAQ software to measure the vertical thrust

Figure 11. Vertical thrust measurement setup.



(a)



(b)

Figure 12. FW-MAV from -60° (a) to 120° (b) for vertical thrust measurement.

3. Results

In this section, the results of wing sizing, prototype fabrication, and analysis are presented. The onboard avionics and their connection are also illustrated in detail. The thrust generation performance of the fabricated wings using both methods are compared between themselves as well as with an off-of-shell bird model wing and are discussed.

3.1. Wing Sizing Result

3.1.1. Step 1—Defining the Mission

It was decided that the mission would be carried out indoors and the flight class of the flapping wing was MAV. The values of each parameter are tabulated in Table 4.

Table 4. Atmospheric parameter at flying place.

Parameter	Symbol	Value
Acceleration of gravity (m/s^2)	g	9.78
Air Temperature ($^{\circ}\text{C}$)	T_a	14.98
Air Density (kg/m^3)	ρ	1.226
Kinematic viscosity (m^2/s)	ν	0.9452
Air Pressure (hPa)	p	1012.639

Note that Step 2 (the flight mode) and Step 3 (wing shape and aspect ratio) have been identified in Section 2 and these values will be used in Steps 4 and 5.

3.1.2. Step 4—Determining the Wing Loading

The required flight parameters to estimate the FW-MAV wing loading are tabulated in Table 5. These values were then used to form the thrust equations for six different flight conditions, as mentioned in Section 2. After that, all curves were plotted on one graph to conduct the constraint analysis to find the optimal wing loading. Figure 13 shows the graph used for the constraint analysis. From Figure 13, it can be noted that the design point (15.20, 0.9925) satisfies all the flight modes' constraints. This is because this point has the minimum thrust loading that provides enough thrust for all six cases. For that, the maximum wing loading which satisfies all constraint is 15.20 N/mm^2 and will be used after Step 5 to calculate the required wing surface area.

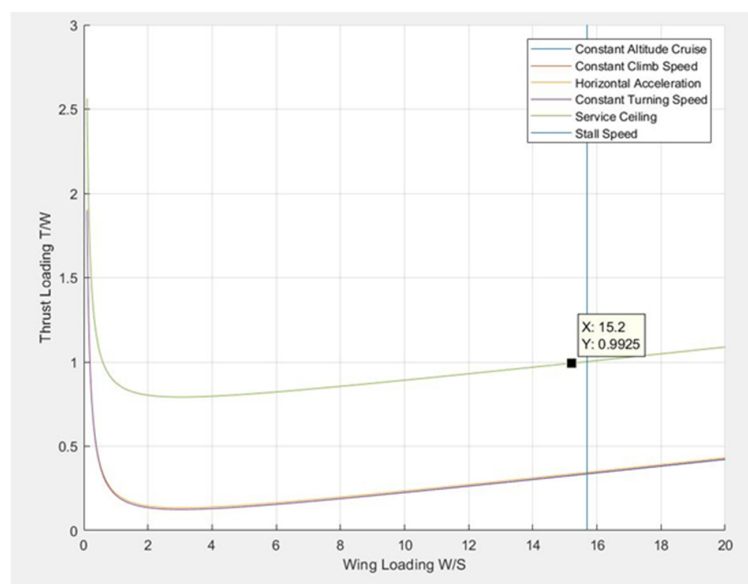


Figure 13. Graph of thrust loading against wing loading for different flight modes.

Table 5. The required flight parameters for wing loading calculation.

Variable	Value	Variable	Value
α	0.999912229	ψ	2.4
k_1	0.1137	C_f	0.007156
e	0.8	U_c	0.8
q	5.517	a_H	0.1

3.1.3. Step 5—Estimating the Electrical and Structural Weights of the FW-MAV

The weights of all electronics are summarized in Table 6. By using this information, the total weight of electrical components W_{Eq} was estimated to be 24.86 g. Next, the weight of the structure, W_{Str} , was also estimated using the statistical method, as presented in Table 2. Based on the ratio of $W_{Str}:W_{Eq} = 38:62$, the estimated structural weight is 15.23 g. After the structural weight and electrical weight were obtained, the total weight of the FW-MAV was estimated to be 40.097g. The weight results are summarized in Table 7.

Table 6. Electronic components' individual mass.

Category	Name	Weight, g	
Electric components used in FW-MAV	Battery, W_B	3.7 V, 70 mAh, 15 C Lithium Polymer battery	2.43
	Payload, W_{PL}	MPU6050 sensor	1.60
		MS5611 Pressure sensor	1.30
		Additional weight for payload such as micro SD breakout board or camera for future use.	3.00
	Avionics, W_{AV}	Arduino Pro Mini328 3.3 V MHz	4.62
		HK-15318B Micro Servo $\times 2$	3.40×2
		FrSky XMR Micro Receiver	0.80
Power Plant, W_{PP}	HW0001498 DC Motor	1.87	
	MOSFET IRFZ44N	2.11	
	1k ohm resistor $\times 3$	0.11×3	

Table 7. Weights and their values.

Weight	Values
Weight of Electrical Components, W_{Eq}	24.86 g
Weight of structure, W_{Str}	15.23 g
Total Weight, W_{To}	40.097 g

After the values of total MAV weight and the wing loading were obtained from Steps 4 and 5, the total wing area was calculated. With known values of total wing area and aspect ratio, the wingspan could be calculated. The length of the wingspan calculated above satisfied all the constraints for different flight modes. By using the wingspan, taper ratio, and the total wing area, a trapezoidal shaped wing with root chord length, C_r of 100 mm was finalized, as shown in Table 8. The tip chord length was estimated as 55 mm. Thus, a pair of flapping wings with 300.0 mm wingspan, 100.0 mm root chord and 55.0 mm tip chord were used on the actual prototype. The wing sizing parameters are shown in Figure 14.

Table 8. All wing sizing parameters and their values.

Wing Sizing Parameters	Values
Total Wing Area, S_w	25,796 mm ²
Wing Aspect Ratio, AR	3.50
Wingspan, b	300.48 mm
Taper Ratio, λ	0.55
Wing tip chord length, c_t	55 mm
Wing root chord length, c_r	100 mm

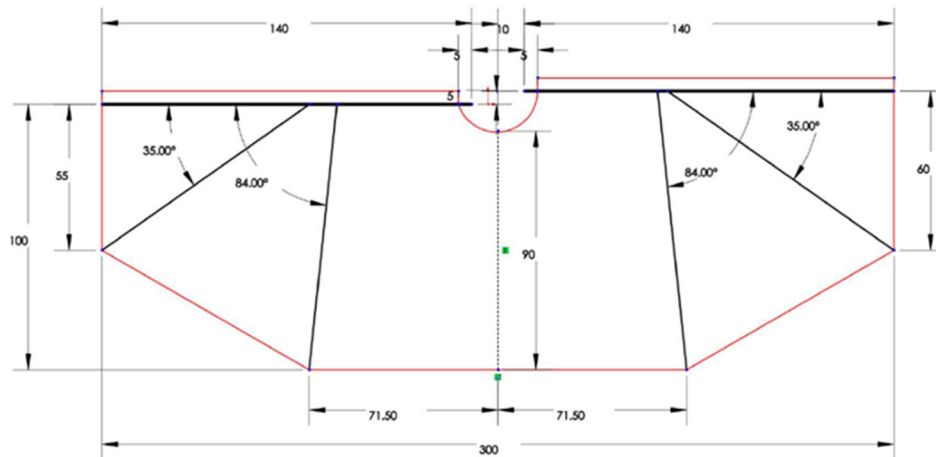


Figure 14. 2D wing drawing and size (in mm).

3.2. Gear Ratio and Flapping Frequencies

The overall gear ratio for the crank-shaft mechanism, $GR_{Mechanism}$, was calculated with $\frac{40}{7} \cdot \frac{40}{9} = 25.40$. $GR_{Mechanism} = 25.40$ means that for every revolution the main gear makes the motor pinion turns and completes 25.40 revolutions. The illustration of the crank-shaft gear combination is shown in Figure 15. When the brushed motor turns at 35,000 rpm, it produces 583.33 revolutions per second. Since the motor pinion has to turn 25.40 revolutions to complete one flapping cycle of the wing, by dividing motor turn rate by the overall gear ratio, the FW-MAV maximum flapping frequency is 22.97 Hz. Using a similar methodology, the minimum flapping frequency is zero when there is no current flowing to the brushed motor. The flapping frequency can vary by controlling the voltage using a metal-oxide semiconductor field-effect transistor (MOSFET). For FW-MAVs, the flapping frequency can be increased to the maximum by increasing the throttle on the remote-control transmitter until the maximum throttle.

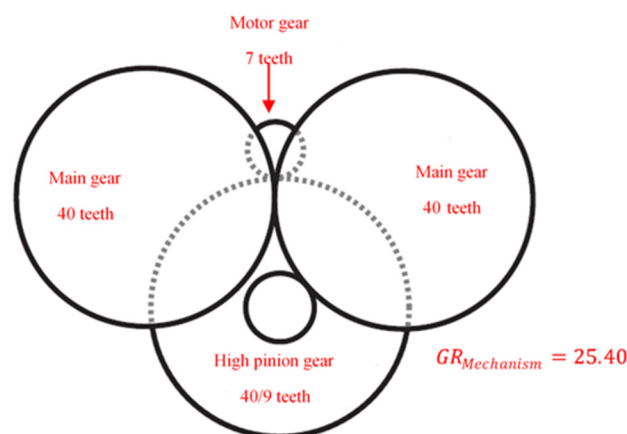


Figure 15. Crank-shaft mechanism with a gear ratio.

3.3. Avionic System

The avionics used on the MAV includes a DC motor, a 3.7 V 70 mAh lithium polymer (LiPo) battery, an Arduino Pro Mini microcontroller, a MPU-6050 IMU sensor, a MS6511 atmospheric pressure sensor, two HK-15318B micro servos, a Frsky XMR receiver, a 1k Ω resistor, and a MOSFET. The system is controlled using a TaranixQ-X7 transmitter. The main criteria of selecting these components are the weight, size, and compatibility of each avionic to the whole system. Figure 16 reveals the overall system architecture of the FW-MAV. All six pulse width modulation (PWM) pins are utilized for the analog control by digital means. The FrSky XMR receiver sends an input signal to the Arduino Pro Mini (via input pin 5, 6, 11) and controls the motor and two servos (via output pin 3, 9, 10). The communication protocol used between Arduino Pro Mini and two sensors are connected through I2C which are pin A5 (clock signal) and A4 (data signal). The avionics system is presented in detail with the functionality of each component in Table A1 in Appendix A.

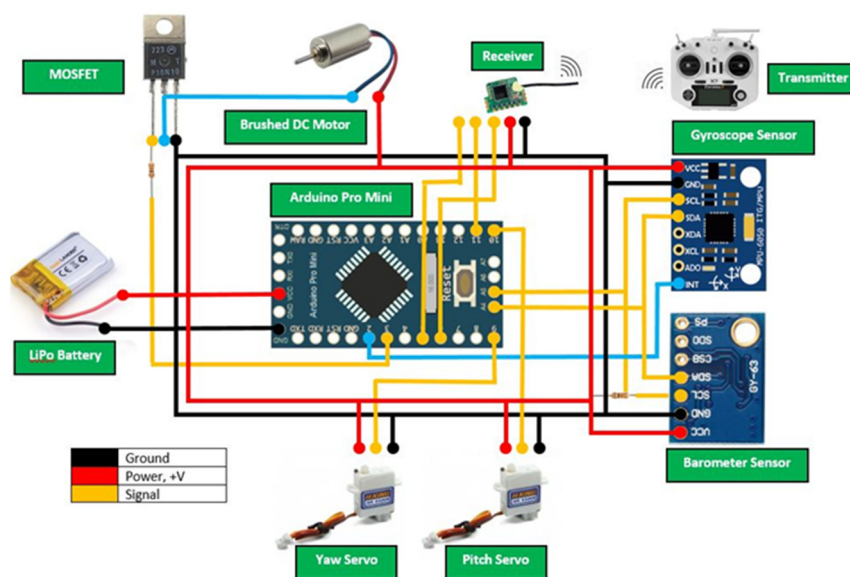


Figure 16. FW-MAV wiring diagram.

3.4. Fabricated Prototype

Figure 17 shows the FW-MAV prototype in front, top, and side views. The onboard avionics and tails are also presented in Figure 17. The overall mass of the FW-MAV is 36.9 g. The prototype assembly began with the avionics soldering followed by adhering the strip board onto the fuselage. After that, the tail, which was built with depron foam, was glued onto the rear end of the fuselage. Finally, the wing was inserted on the gear system to complete the assembling process. A tethered flight test was conducted to check the movements of the FW-MAV in terms of flapping, yawing, and pitching [27].

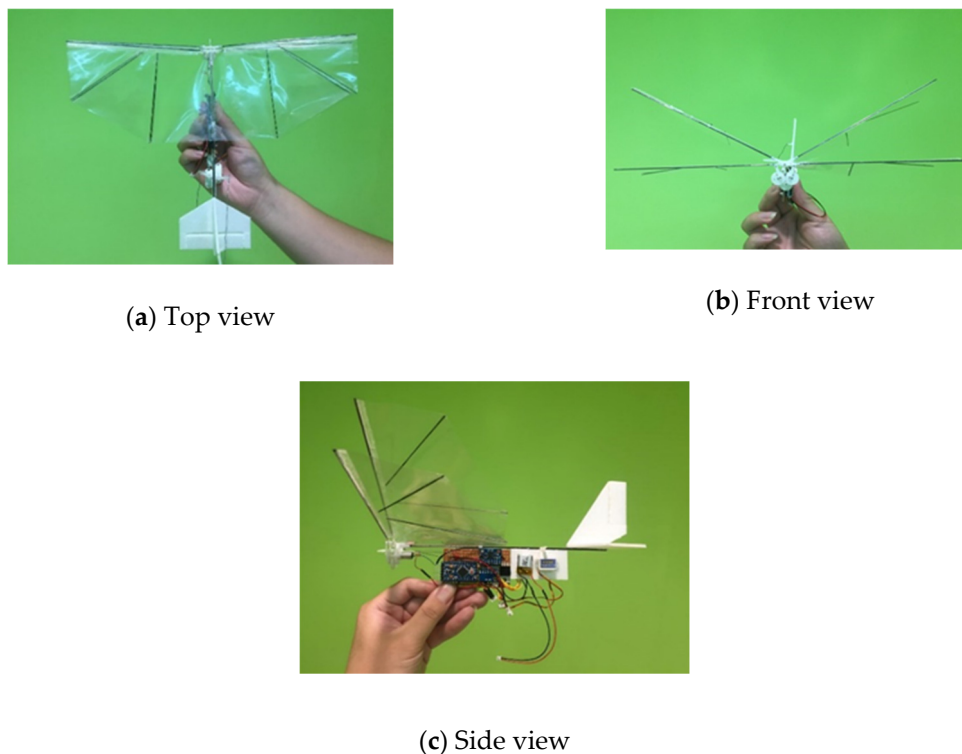


Figure 17. FW-MAV prototype. (a) Top view, (b) Front view, and (c) Side view of the FW-MAV.

3.5. Vertical Thrust Measurement Result

The vertical thrust data for the wings fabricated from the traditional and advanced methods at different pitch angles were measured. To check the performance of both wings with other type of wing, an off-the-shell elliptical bird model wing was included in the comparison. Each of these vertical thrust datum represent the average value calculated from a set of raw data which were obtained from the load cell.

Figure 18 shows the thrust measurement of wing 1, which was fabricated using the traditional method, and wing 2, which was made using the advanced method. The standard deviation of each raw data set used to calculate the average thrust value is also plotted in Figure 18 using error bars. There is an obvious trend for the FW-MAV vertical thrust generation. The thrust generation became lesser as the pitch angle was decreased from 0° to -60° . Notice that there was a drastic decrease in the thrust when the FW-MAV flapped at negative pitch angles. This happened at the pitch angle of -10° , where wing 1 suffered a 16.7% thrust reduction and wing 2 lost 13.3% of its thrust compared with the thrust values at a pitch angle of 0° . Going towards the right-hand side, when the pitch angle was increased from 0° to 120° , the FW-MAV vertical thrust reached the highest value at the pitch angle of 10° , then gradually decreased all the way to 120° regardless of which wing was used.

The vertical thrusts generated by wing 2 are always higher than those of wing 1 at all considered pitch angles. At the pitch angle of 10° , the FW-MAV with wing 2 has the highest vertical thrust value of 86.75 g, compared to the FW-MAV with wing 1, which has 80.875 g. The difference in values is believed to be caused by the overall wing tension throughout the wing contour. In the traditional fabrication method, the PET film was fixed above the 2D drawing using the tape. This process of pulling and pasting has exerted some tensional forces on the PET film when the wings performed clap-and-fling. On the other hand, wing 2, which was fabricated by placing the PET film on the vacuum mold, possessed lower tension forces. When the wings clapped and pushed the air out, the wing, which has no tension force, would create a more streamline and smooth airflow. This is similar during the fling motion, when two wings started to separate and create a low-pressure region between the wing gap.

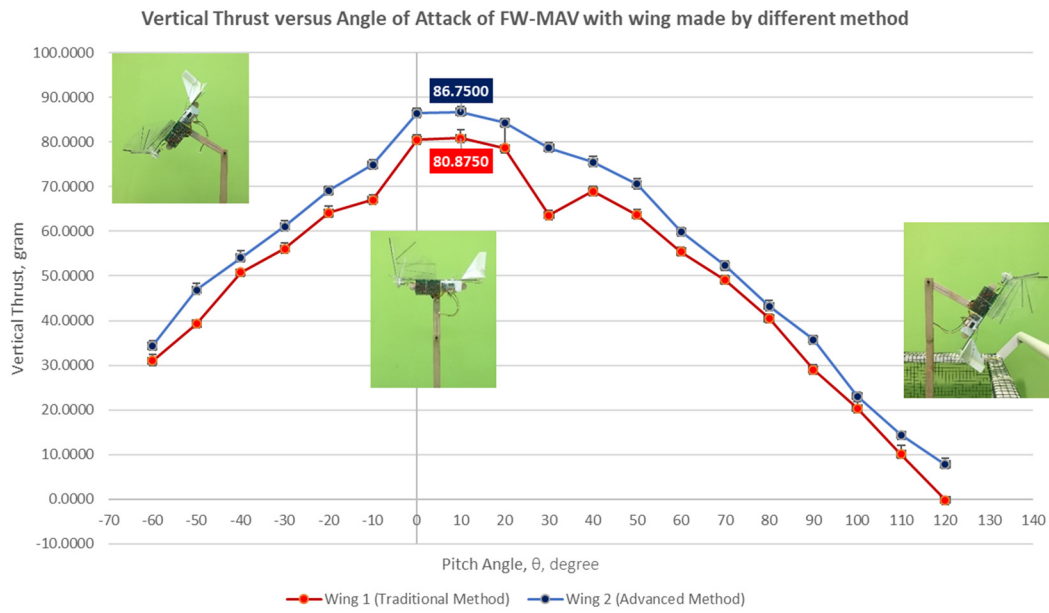


Figure 18. Graph of vertical thrust versus pitch angle for wing 1 and wing 2.

Table 9 summarizes the specification of wing 1, wing 2 and the bird model wing. In Figure 19, it can be clearly seen that the maximum vertical thrust generated by the bird model wing was lower than that of the wing 2 at the pitch angle of 10°. This is because wing 2 has eight 0.5 mm stiffeners (i.e., four on the upper wing and four on the lower wing) which give the PET film more rigidity to allow the wings to perform a regular dynamic twist for every flapping motion. However, the bird model wing produced larger vertical thrust values at higher pitch angles, that is, from 30° onwards. The elliptical shape characteristics of the bird model wing could have contributed to this result.

Table 9. Specifications of wing 1, wing 2 and the bird model wing.

Wings	Dimensions	Mass	Shape	Stiffeners
 Wing 1 (Traditional Method)	30.0 cm × 10.5 cm	2.81 g	Trapezoidal	Yes
 Wing 2 (Advanced Method)	30.0 cm × 10.5 cm	2.87 g	Trapezoidal	Yes
 Bird Model Wing	28.0 cm × 9.5 cm	1.68 g	Elliptical	No



Figure 19. Graph of vertical thrust versus pitch angle for the bird model wing and wing 2.

4. Conclusions

An X-wing flapping-wing Micro Air Vehicle (FW-MAV) with a better payload carrying capability is designed, fabricated, and analyzed in this paper. The wing design process was performed using a systematic approach to determine essential wing parameters. Two pairs of wings were fabricated using the traditional and advance mold methods. A prototype of FW-MAV was built by integrating the avionic system and assembling it with the wing, tail, fuselage and gear system. The final mass of the FW-MAV was 36.9 g with a wingspan of 30.0 cm. Apart from that, thrust measurement experiments were conducted using the load cell setup to measure the vertical thrust generated by the FW-MAV for different wings. By comparing these measurements, the results conclude that the FW-MAV produces the highest thrust at the pitch angle of 10°, and most importantly, wing 2 produces the highest vertical thrust of 86.75 g, compared to that of the wing 1 and the bird model wing. This preliminary study on designing a FW-MAV opens up opportunities to further investigate the feasibility of a fully autonomous flight of FW-MAV by designing a controller for this MAV.

Author Contributions: Conceptualization, H.W.H.; Methodology, B.H.C.; Software, B.H.C.; Validation, B.H.C.; Formal analysis, B.H.C.; Investigation, H.W.H. and E.A.B.; Resources, H.W.H.; Data curation, B.H.C.; Writing-original draft, B.H.C.; Writing-review & editing, H.W.H.; Visualization, B.H.C.; Supervision, H.W.H.; Project administration, H.W.H. and E.A.B.; Funding acquisition, H.W.H.

Acknowledgments: The authors would like to thank Universiti Sains Malaysia (USM) for providing the Short Term Research Grant Scheme (304/PAERO/6315113).

Conflicts of Interest: The authors declare no conflict of interest.

Appendix A

Table A1. The avionics system with the functionality of each component.

Item	Parameter	Value
 <p>DC Micro Brushed Motor Function: to generate torque to flap the wing</p>	Model	HW0001498
	Motor diameter	6.0 mm
	Motor length	14.0 mm
	Output shaft diameter	0.8 mm
	Output shaft length	5.0 mm
	Motor speed	35,000 RPM
	Voltage	DC 3.7 V
	Current	0.1 Amps
	Service life	10,000
	Mass	1.87 grams

Table A1. Cont.

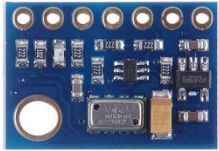
Item	Parameter	Value
 <p>Micro servos <i>Function: to deflect the elevator and rudder</i></p>	Model	HobbyKing™ HK-15318B
	Mass	3.4 g
	Size	8* 20* 23 mm
	Operating Speed	0.09 s/60 degrees
	Stall Torque	0.10 kg/cm
	Operating Voltage	2.8 V~4.2 V
	Battery Plug	1S capable JST .25 Pitch
 <p>LiPo Battery <i>Function: to provide power source</i></p>	Model	LiPo Rechargeable Battery
	Capacity	70 mAh
	Voltage	3.7 V
	Cycle life	500~700 cycles
	Mass	2.43 g (including wire)
	Dimensions	4.0* 14* 20 mm
	Balance Plug	JST
 <p>MOSFET <i>Function: to regulate voltage</i></p>	Model	IRFZ44N Power MOSFET
	Type	N – Channel
	Maximum Drain-Source	55.0 V
	Maximum Gate-Source	10.0 V
	Maximum Gate-Threshold	4.0 V
	Mass	2.11 g
 <p>Arduino Pro Mini <i>Function: to process input and sensor signals and send output signals and serve as the autopilot</i></p>	Model	ATmega328
	Operating Voltage	3.3 V
	Board Power Supply	3.35 V~12.0 V
	Maximum current drawn	200 mA
	PWM Pins	6
	Analog Input Pins	6
	Flash Memory	32 Kbytes
	Clock Speed	8 MHz
	I2C	1
	PWM Pins	6
	Dimension	18 mm * 33 mm
	Mass	4.62 g (includes pin headers)
	 <p>Gyroscope + Accelerometer Sensor <i>Function: to measure rotational rates and linear accelerations</i></p>	Model
Chip		MPU-6050
Operating Voltage		3.0 V~5.0 V
Dimensions		20.3 mm* 15.6 mm
Mass		1.60 g
Gyroscope range		+ 250 500 1000 2000 degree/s
Acceleration range		± 2 ± 4 ± 8 ± 16 g
Communication		I2C
Pin Pitch	2.54 mm	
 <p>Atmospheric Height Sensor <i>Function: to measure the altitude</i></p>	Model	MS5611 Barometric Module
	Chip	MS5611
	Operating Voltage	3.0 V~5.0 V
	Dimensions	19 mm* 13 mm
	Mass	1.30 g
	Operating temperature	-40~+85 °C
Communication	I2C/SPI	

Table A1. Cont.

Item	Parameter	Value
 <p>Receiver Function: to communicate with the transmitter</p>	Model	FrSky XMR micro receiver
	Frequency band	2.4 GHz
	Mass	0.8 g
	Operating Current	20 mA @ 5.0 V
	Operating Voltage	3.5 V~10.0 V
	Operating Range	300 m
	Number of Channels	1~6 channel
	Dimension	15* 14* 3.5 mm
	Weight	0.74 g
	Compatibility	Transmitter D16 modules mode
 <p>Transmitter Function: to communicate with the receiver</p>	Model	Taranis Q-X7
	Frequency band	2.4~2.4835 GHz
	Number of Channels	16~32 channels
	Operating Temperature	-10~60 °C
	Operating Current	210 mA
	Operating voltage	6.0 V~15.0 V
	Flash Memory	16 MB

References

- Mwongera, V.M. A review of Flapping Wing MAV modelling. *Int. J. Aeronaut. Sci. Aerosp. Res.* **2015**, *2*, 27–36.
- Tang, J.; Sun, J.; Lu, C.; Lao, S. Optimized artificial potential field algorithm to multi-unmanned aerial vehicle coordinated trajectory planning and collision avoidance in three-dimensional environment. *Proc. Inst. Mech. Eng. Part G J. Aerosp. Eng.* **2019**. [[CrossRef](#)]
- D'Andrea, R. Guest editorial can drones deliver? *IEEE Trans. Autom. Sci. Eng.* **2014**, *11*, 647–648. [[CrossRef](#)]
- Nakata, T.; Liu, H.; Tanaka, Y.; Nishihashi, N.; Wang, X.; Sato, A. Aerodynamics of a bio-inspired flexible flapping-wing micro air vehicle. *Bioinspir. Biomim.* **2011**, *6*, 045002. [[CrossRef](#)] [[PubMed](#)]
- Armanini, S.F.; De Visser, C.C.; De Croon, G.C.H.E.; Mulder, M. Time-varying model identification of flapping-wing vehicle dynamics using flight data. *J. Guid. Control Dyn.* **2015**, *38*, 526–541. [[CrossRef](#)]
- Armanini, S.F.; Caetano, J.V.; De Croon, G.C.H.E.; De Visser, C.C.; Mulder, M. Quasi-steady aerodynamic model of clap-and-fling flapping MAV and validation using free-flight data. *Bioinspir. Biomim.* **2016**, *11*, 046002. [[CrossRef](#)] [[PubMed](#)]
- Shyy, W.; Aono, H.; Kang, C.K.; Liu, H. *An Introduction to Flapping Wing Aerodynamics*; Cambridge University Press: New York, NY, USA, 2013; Volume 37.
- Weis-Fogh, T. Quick estimates of flight fitness in hovering animals, including novel mechanisms for lift production. *J. Exp. Biol.* **1973**, *59*, 169–230.
- Ellington, C.P.; Van Den Berg, C.; Willmott, A.P.; Thomas, A.L. Leading-edge vortices in insect flight. *Nature* **1996**, *384*, 626. [[CrossRef](#)]
- Dickinson, M.H.; Lehmann, F.O.; Sane, S.P. Wing rotation and the aerodynamic basis of insect flight. *Science* **1999**, *284*, 1954–1960. [[CrossRef](#)] [[PubMed](#)]
- Sane, S.P. The aerodynamics of insect flight. *J. Exp. Biol.* **2003**, *206*, 4191–4208. [[CrossRef](#)] [[PubMed](#)]
- Wood, R.J. The first takeoff of a biologically inspired at-scale robotic insect. *IEEE Trans. Robot.* **2008**, *24*, 341–347. [[CrossRef](#)]
- Pister, K.S.; Judy, M.W.; Burgett, S.R.; Fearing, R.S. Microfabricated hinges. *Sens. Actuators A Phys.* **1992**, *33*, 249–256. [[CrossRef](#)]
- Trimmer, W.S. Microrobots and micromechanical systems. *Sens. Actuators* **1989**, *19*, 267–287. [[CrossRef](#)]
- Keennon, M.; Klingebiel, K.; Won, H.; Andriukov, A. Development of the Nano Hummingbird: A tailless flapping wing micro air vehicle. In Proceedings of the 50th AIAA Aerospace Sciences Meeting Including the New Horizons Forum and Aerospace Exposition, Nashville, TN, USA, 9–12 January 2012; pp. 1–17.

16. Phan, H.V.; Kang, T.; Park, H.C. Design and stable flight of a 21 g insect-like tailless flapping wing micro air vehicle with angular rates feedback control. *Bioinspir. Biomim.* **2017**, *12*, 036006. [[CrossRef](#)] [[PubMed](#)]
17. Groen, M.; Bruggeman, B.; Remes, B.; Ruijsink, R.; Van Oudheusden, B.W.; Bijl, H. Improving flight performance of the flapping wing MAV DelFly II. In Proceedings of the Int. Micro Air Vehicle Conf. and Competition (IMAV 2010), Braunschweig, Germany, 6–8 July 2010.
18. Karásek, M.; Muijres, F.T.; De Wagter, C.; Remes, B.D.; de Croon, G.C. A tailless aerial robotic flapper reveals that flies use torque coupling in rapid banked turns. *Science* **2018**, *361*, 1089–1094. [[CrossRef](#)] [[PubMed](#)]
19. Nguyen, Q.V.; Chan, W.L.; Debiasi, M. Experimental investigation of wing flexibility on force generation of a hovering flapping wing micro air vehicle with double wing clap-and-fling effects. *Int. J. Micro Air Veh.* **2017**, *9*, 187–197. [[CrossRef](#)]
20. Phan, H.V.; Park, H.C. Design and evaluation of a deformable wing configuration for economical hovering flight of an insect-like tailless flying robot. *Bioinspir. Biomim.* **2018**, *13*, 036009. [[CrossRef](#)] [[PubMed](#)]
21. Nan, Y.; Karásek, M.; Lalami, M.E.; Preumont, A. Experimental optimization of wing shape for a hummingbird-like flapping wing micro air vehicle. *Bioinspir. Biomim.* **2017**, *12*, 026010. [[CrossRef](#)] [[PubMed](#)]
22. Bruggeman, B. Improving Flight Performance of DelFly II in Hover by Improving Wing Design and Driving Mechanism. Master's Thesis, Delft University of Technology, Delft, The Nederland, 2010.
23. Yang, W.; Wang, L.; Song, B. Dove: A biomimetic flapping-wing micro air vehicle. *Int. J. Micro Air Veh.* **2018**, *10*, 70–84. [[CrossRef](#)]
24. Nam, T. A generalized sizing method for revolutionary concepts under probabilistic design constraints. Ph.D. Thesis, Georgia Institute of Technology, Atlanta, GA, USA, 2007.
25. Silin, D. Aerodynamics and Flight Performance of Flapping Wing Micro Air Vehicles. Ph.D. Thesis, University of Arizona, Tucson, AZ, USA, 2010.
26. Hassanalian, M.; Abdelkefi, A. Methodologies for weight estimation of fixed and flapping wing micro air vehicles. *Meccanica* **2017**, *52*, 2047–2068. [[CrossRef](#)]
27. FW-MAV Tethered Flight Test. Available online: <https://youtu.be/qfACJa0LJOc> (accessed on 2 August 2019).



© 2019 by the authors. Licensee MDPI, Basel, Switzerland. This article is an open access article distributed under the terms and conditions of the Creative Commons Attribution (CC BY) license (<http://creativecommons.org/licenses/by/4.0/>).